IEEE Photonics Journal
An IEEE Photonics Society Publication

Open Access

Wavelength-Selective Infrared Metasurface Absorber for Multispectral Thermal Detection

Volume 7, Number 6, December 2015

Joo-Yun Jung
Jihye Lee
Dae-Geun Choi
Jun-Hyuk Choi
Jun-Ho Jeong
Eung-Sug Lee
Dean P. Neikirk

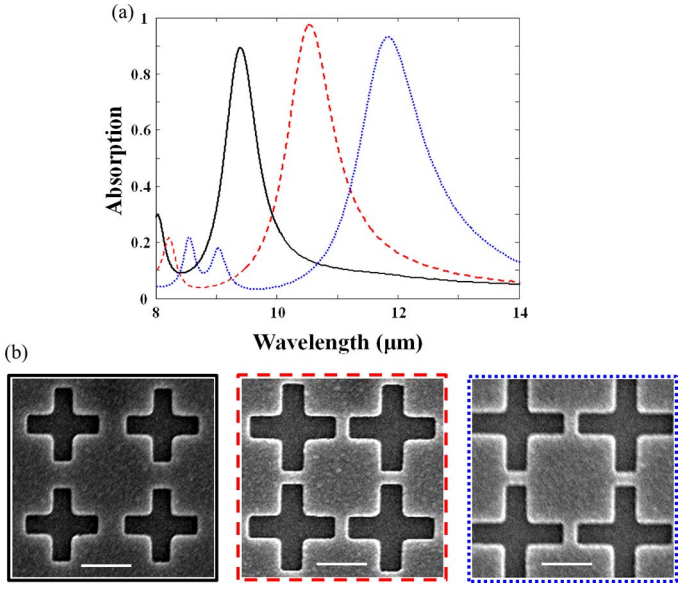

DOI: 10.1109/JPHOT.2015.2504975
1943-0655

IEEE photonics SOCIETY

IEEE

Wavelength-Selective Infrared Metasurface Absorber for Multispectral Thermal Detection

Joo-Yun Jung,[1] Jihye Lee,[1] Dae-Geun Choi,[1] Jun-Hyuk Choi,[1] Jun-Ho Jeong,[1] Eung-Sug Lee,[1] and Dean P. Neikirk[2]

[1]Department of Nano Manufacturing Technology, Korea Institute of Machinery and Materials, Daejeon 305-343, Korea
[2]Microelectronics Research Center, Department of Electrical and Computer Engineering, The University of Texas at Austin, Austin, TX 78712-1024 USA

DOI: 10.1109/JPHOT.2015.2504975

Manuscript received October 15, 2015; revised November 28, 2015; accepted November 30, 2015. Date of publication December 4, 2015; date of current version December 15, 2015. This work was supported by the Center for Advanced Meta-Materials (CAMM) funded by the Ministry of Science, ICT and Future Planning as Global Frontier Project (CAMM-No. 2014M3A6B3063707) and the Basic Science Research Program (2011-0028585) funded by the National Research Foundation of Korea (NRF). This work was also supported by the Korea Institute of Machinery and Materials (KIMM) under research Grant (NK188E). Corresponding authors: J.-Y. Jung and D. P. Neikirk (e-mail: jjy2121@kimm.re.kr; neikirk@mail.utexas.edu).

Abstract: A wavelength-selective metasurface absorber suitable for use in multispectral microbolometer focal plane arrays in the long-wavelength infrared (LWIR) region is theoretically and experimentally investigated. We show that a thin metal metasurface, which is characterized by effective surface impedance, as an absorbing layer can be integrated with an asymmetric Fabry–Pérot cavity to construct a wavelength-selective perfect absorber. The absorbed infrared energy is mainly dissipated in a thin metal metasurface, in contrast to a multilayer metamaterial absorber. The calculated and experimental spectral responses of the metasurface absorbers show excellent wavelength-selective narrowband absorption to allow multispectral imaging in LWIR.

Index Terms: Metamaterials, subwavelength structures, thermal infrared (IR) detectors.

1. Introduction

Uncooled infrared microbolometer focal plane arrays have been used in low-cost infrared thermal imaging systems for many applications such as night vision, surveillance, thermography, and firefighting. The absorption of incident infrared radiation in long wavelength infrared (LWIR) microbolometers causes an increase in the temperature of the thermally isolated bolometric layer, which is then converted into electrical signals. In order to enhance the absorption of incident radiation, conventional LWIR microbolometers normally use a broadband Salisbury screen absorber, which consists of a single thin resistive absorbing layer placed a quarter-wavelength in front of a metal mirror layer. The development of multispectral microbolometers, which are capable of allowing better recognition and discrimination of objects compared to conventional microbolometers, is highly desirable [1]. For multispectral response, wavelength-selective narrowband absorption in the LWIR band is necessary. Several other approaches for producing a wavelength-selective microbolometer absorber, such as antenna-coupled microbolometers [2],

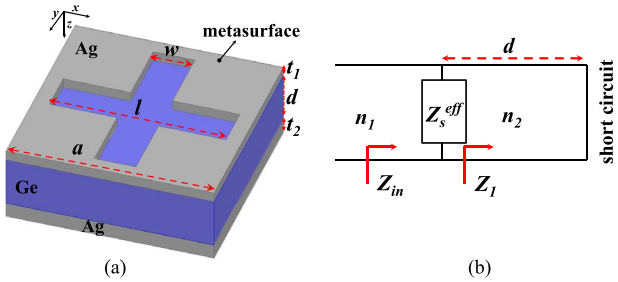

Fig. 1. (a) Schematic of a single unit of a wavelength-selective metasurface absorber. (b) Equivalent transmission line.

modified Fabry-Perot cavity absorber [3], [4], plasmonic structure [5], and microbolometers with a metamaterial absorber [6]–[9], have been presented. Particularly, the spectral response of a metamaterial absorber, which consists of a sub-wavelength-sized patterned metal array on top of a continuous metal layer separated by a thin dielectric layer (much less than a quarter-wavelength thick), can achieve excellent wavelength-selective narrowband absorption [10]–[15]. In contrast to the Salisbury screen absorber, the electromagnetic energy loss of a metamaterial absorber is dissipated in either two-metal layers [14] or a lossy thin dielectric layer between the metal layers [10], [12], [13] because the near-field coupling of metal-dielectric-metal layers determines the behavior of the resonant absorption. For a sensitive microbolometer performance, the absorbing membranes of a microbolometer pixel, which mainly consist of a resistive absorbing layer, bolometric layer, and a mechanical support layer, should be thermally isolated, i.e., the absorbing membranes are suspended over the metal mirror layer on the substrate. In such microbolometers with a multilayer metamaterial absorber, the additional layers of the absorbing membranes can increase the thermal mass of the microbolometer and result in decreased response speed of the microbolometer.

Recently, metasurfaces, which are a kind of thin metamaterial structure comprising arrays of sub-wavelength-sized resonators and can produce abrupt alteration of the phase and amplitude of incident light at a metasurface, provide a novel solution for tailoring spectral response [16]–[21]. Thin metal or graphene metasurfaces with an appropriate effective surface impedance have been used as a component of narrowband [22], broadband [23], or a tunable so-called perfect absorbers [24]–[27].

In this paper, a metasurface absorber designed using transmission line theory and an effective surface impedance approach is experimentally and theoretically investigated. An analytical solution to design an optimized surface impedance of the metasurface for achieving near-perfect absorption by the metasurface absorber is also investigated. The optimized metasurface absorbers, which have multispectral thermal detection capability, produce wavelength-selective narrowband absorption in the LWIR band. The infrared absorption energy absorbed by the metasurface absorber is mainly dissipated in a single-layer thin (50 nm) metal metasurface, in contrast to a multilayer metamaterial absorber. Finally, the conceptual structure of a wavelength-selective microbolometer pixel using the proposed metasurface absorber is investigated.

2. Results and Discussion

The concept of constructing a wavelength-selective narrowband absorber is based on the integration of the metasurface and the classical Salisbury screen absorber forming an asymmetric Fabry-Perot cavity. Fig. 1(a) shows a schematic of the wavelength-selective metasurface absorber, consisting of a thin silver (Ag) layer (t_1) perforated with an array of cross patterned holes as a metasurface, a germanium (Ge) dielectric spacer layer (d), and a bottom Ag mirror layer (t_2). The metasurface, which has three design parameters, namely, the dimensions of the cross holes (length l and width w) and the array period (a), has both an electric dipole resonance as a slot antenna and a bandpass transmittance spectral response. Since the thickness of the

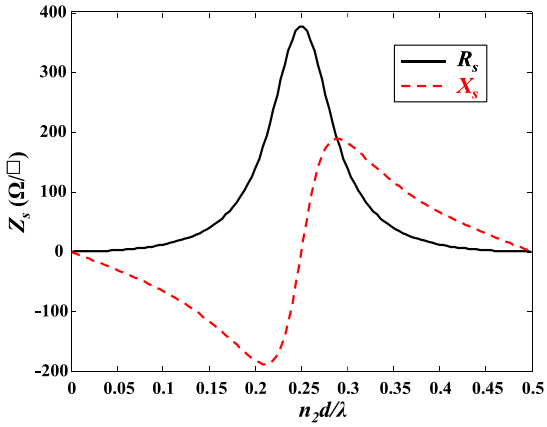

Fig. 2. Ideal surface impedance of a metasurface for perfect absorption as a function of the effective thickness of the dielectric layer $(n_2 d/\lambda)$.

metasurface is much smaller than the operation wavelength, the metasurface can be considered as a resistive sheet with an effective surface impedance (Z_s^{eff}). The transmission line model of the metasurface absorber is shown in Fig. 1(b). The input impedance Z_{in} is defined as

$$Z_{\text{in}} = \frac{jZ_s^{\text{eff}} Z_d \tan(\beta_d d)}{Z_s^{\text{eff}} + jZ_d \tan(\beta_d d)} \tag{1}$$

and the reflection coefficient Γ is defined as

$$\Gamma = \frac{Z_{\text{in}} - Z_0}{Z_{\text{in}} + Z_0} \tag{2}$$

where Z_0 and $Z_d = Z_0/n_2$ are the characteristic impedances of free space and the dielectric layer, n_2 is the refractive index of the dielectric layer, and $\beta_d = (2\pi n_2)/\lambda$ is the propagation constant. The absorption of a metasurface absorber can be determined using

$$A = 1 - |\Gamma|^2. \tag{3}$$

From (1) and (2), the analytical solution for an ideal surface impedance of a metasurface required for the perfect absorption condition $(\Gamma = 0)$ can be determined using

$$Z_s^{\text{eff}} = \frac{jZ_0 Z_d \tan(\beta_d d)}{jZ_d \tan(\beta_d d) - Z_0}. \tag{4}$$

The required ideal surface impedance of a metasurface for the perfect absorption as a function of the effective thickness of the dielectric layer $(n_2 d/\lambda)$ is plotted in Fig. 2 using equation (4). When the dielectric layer is a quarter-wavelength thick $(\lambda/4n_2)$, i.e., the effective thickness of the dielectric layer is 0.25, the effective surface impedance of the metasurface should be purely resistive $(R_s^{\text{eff}} = 377\Omega/\square)$ to obtain perfect absorption. These required conditions are equivalent to those of the classical Salisbury screen absorber. Depending on the effective thickness of the dielectric layer, the effective surface impedance of a metasurface can be designed using this analytical solution.

To calculate the absorption of the metasurface absorber shown in Fig. 1, the effective surface impedance of metasurface is required. The numerical method and formulas to retrieve the effective electric surface conductivity $(\sigma_s^{\text{eff}} = 1/Z_s^{\text{eff}})$ of thin metal and graphene metasurfaces are adopted to calculate the effective surface impedance of the metasurface [18], [24], [28]. Normal incidence of electromagnetic waves on the electric metasurface in the asymmetric dielectric

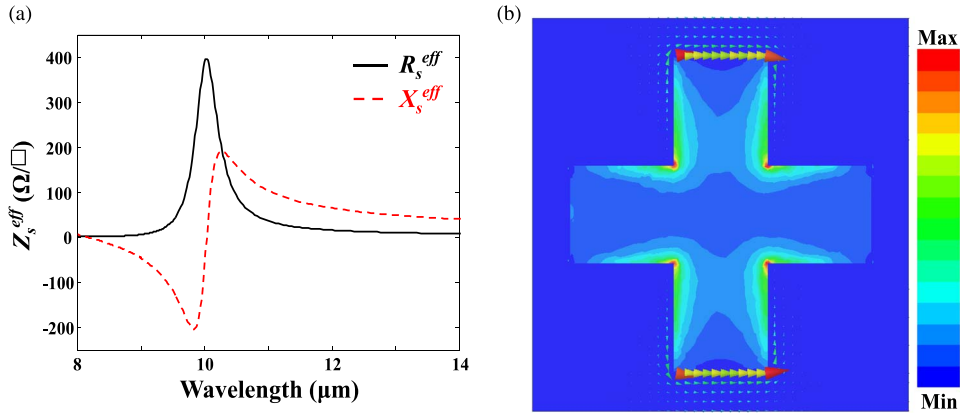

Fig. 3. (a) Retrieved effective surface impedance of the metasurface. (b) Simulated magnitude of electric field and current distribution on top of the metasurface at resonance wavelength.

layers is considered in this situation. The effective surface conductivity of a metasurface can be expressed as [24]

$$\sigma_s^{\text{eff}} Z_0 = \frac{2}{S_{21}} \sqrt{n_1 n_2} - (n_1 + n_2) \tag{5}$$

where n_1 and n_2 are the refractive indices of the free space and Ge layer, respectively. The S21-parameter represents the transmission coefficient for a wave coming from free space (n_1). The S21-parameter is simulated using a commercial numerical software HFSS. The normal incident plane wave with the electric field polarization along the x-direction excites a single unit of metasurface with a periodic boundary condition in the x-y plane. The dielectric Ge layer is almost lossless and non-dispersive in the LWIR band and is assumed to have $n_2 = 4$ [29]. The complex dielectric constant of the bulk Ag layer in the LWIR band is described by the Drude model with the plasma frequency $\omega_p = 1.37 \times 1016$ rad/s and a damping constant $y = 2.74 \times 1013$ rad/s [30]. The damping constant of the thin Ag metal metasurface (t_1) is higher than that of bulk Ag metal due to the surface scattering and grain boundary effects in thin metal layer [11], [31]. Simulated spectral responses with three times the damping constant of bulk Ag provide the best agreement with the measured spectral responses, and so that value is used for the simulation. The simulated metasurface has design parameters of $a = 2.0$ μm, $l = 1.6$ μm, $w = 0.5$ μm, and $t_1 = 50$ nm. The retrieved effective surface impedance of the metasurface using (5) is shown in Fig. 3(a), and it clearly shows a resonant response around a wavelength of 10 μm. The effective surface impedance is purely resistive $(R_s^{\text{eff}} = 395\ \Omega/\square)$ at the resonance wavelength of 10.03 μm. To further clarify the resonant response of the retrieved effective surface impedance, the simulated electric field and current distribution on top of the metasurface at the resonance wavelength is also shown in Fig. 3(b). For the x-direction polarization, the longitudinal rectangular hole along the polarization direction can be considered as a slot antenna. The interaction between the slot antenna and the electromagnetic wave results in a concentrated electric field around the edge of the center cross hole and strong current flow around cross hole, which demonstrates a strong electric dipole resonance. Therefore, the resonant response of the retrieved effective surface impedance is due to the electric dipole resonance.

To achieve near-unity absorption for the metasurface with effective surface resistance $R_s^{\text{eff}} = 395\ \Omega/\square$, which is similar to Z_0, at the wavelength of 10 μm, the absorption of the metasurface absorber with a quarter-wavelength-thick Ge spacer layer $(d = 0.625\ \mu\text{m})$ on the perfect electric conductor (PEC) mirror layer is calculated using transmission line theory. Fig. 4 shows a comparison between the calculated absorption spectral response (black solid) and the simulated spectral response (red dashed), obtained using numerical software HFSS, for a

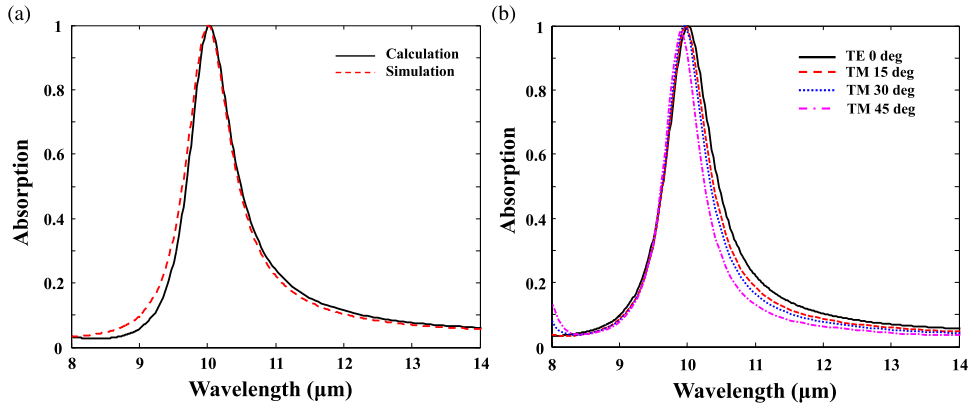

Fig. 4. (a) Calculated (black solid) and simulated (red dashed) absorption spectral responses of a wavelength-selective metasurface absorber. (b) Simulated absorption spectral responses dependence on incident polarization and incident angle.

metasurface absorber with a Ag metal mirror layer instead of a PEC. The result of the calculated spectral response is in excellent agreement with the result of the simulated spectral response and shows excellent wavelength-selective near-unity absorption (99.9%), whose infrared energy is dissipated as ohmic loss in the thin metal metasurface. The simulated integrated power absorption dissipation caused by the thin metal metasurface and the Ag mirror layer are 96.3% and 3.6%, respectively. Since the effective surface impedance of the metasurface changes rapidly, the bandwidth of the metasurface absorber is narrow enough to allow multispectral imaging in the LWIR band. Additional simulation results shown in Fig. 4(b) show that the spectral responses of metasurface absorber for both TE and TM modes are identical and the optical properties of metasurface absorber depend to some extent on the incidence angle. As the incidence angle increases, the resonance peak shifts to shorter wavelength. However, from the perspective of IR microbolometers focal plane arrays used in an imaging system, the absorption at normal incidence is dominant due to the relatively low NA lens (i.e., relatively high f-number) usually used in microbolometer imaging systems.

Fig. 5(a) shows the calculated multispectral responses for three different wavelength-selective metasurface absorbers, which have a common Ge spacer layer thickness d of 0.6 μm and metasurface thickness t_1 of 50 nm. The analytical solution (4) provides the ideal effective surface impedances of each metasurface for the perfect absorption depending on the effective thickness of the dielectric layer $(n_2 d/\lambda)$. The resonance wavelength of the metasurface absorber can be selected through tailoring the dimensions of the metasurface. When the effective thickness of the dielectric layer is 0.242 ($\lambda = 9.9$ μm, $d = 0.6$ μm, and $n_2 = 4$), the ideal effective surface impedance for perfect absorption should be $363.62 - 69.28\text{j}\ \Omega/\square$. However, the retrieved effective surface impedance of the metasurface with dimensions of $a = 2$ μm, $l = 1.45$ μm, and $w = 0.35$ μm is $245.41 - 29.73\text{j}\ \Omega/\square$ at a wavelength of 9.9 μm, as shown in Fig. 5(b). The difference between the ideal and retrieved cases of surface impedance at a wavelength of 9.9 μm implies that the metasurface absorber only exhibits 95.83% absorption (Fig. 5(a), black solid) instead of 100%. For the metasurface with dimensions of $a = 2$ μm, $l = 1.7$ μm, and $w = 0.4$ μm, the retrieved effective surface impedance at a wavelength of 10.83 μm, as shown in Fig. 5(c), is $247.06 - 174.02\text{j}\ \Omega/\square$, which is similar to the ideal effective surface impedance $(247.87 - 178.78\text{j}\ \Omega/\square)$ of the metasurface for perfect absorption when the effective thickness of the dielectric layer is 0.22 ($\lambda = 10.83$ μm, $d = 0.6$ μm, and $n_2 = 4$). The retrieved effective surface impedance of the metasurface with dimensions of $a = 2.2$ μm, $l = 1.9$ μm, and $w = 0.4$ μm at a wavelength of 12.05 μm, as shown in Fig. 5(d), is $139.12 - 169.61\text{j}\ \Omega/\square$, which is also similar to the ideal effective surface impedance $(137.04 - 181.27\text{j}\ \Omega/\square)$ of the metasurface for perfect absorption when the effective thickness of the dielectric layer is 0.199 ($\lambda = 12.05$ μm, $d = 0.6$ μm,

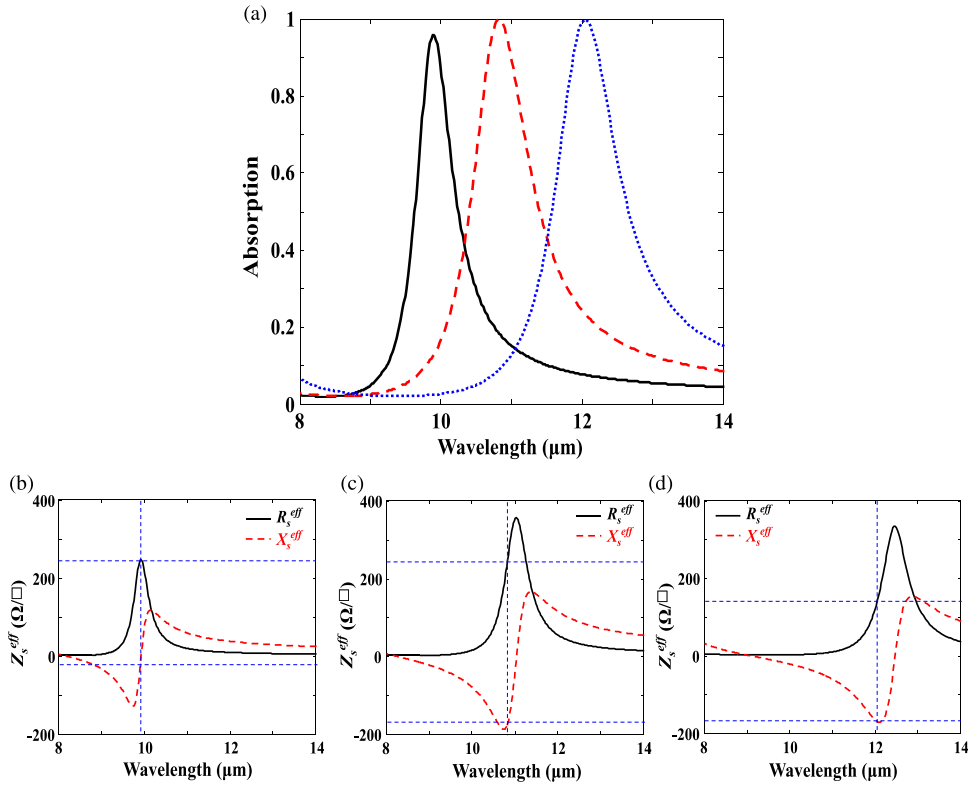

Fig. 5. (a) Calculated spectral responses of three different wavelength-selective metasurface absorbers with a common Ge spacer layer thickness ($d = 0.6$ μm) and metasurface thickness ($t_1 = 50$ nm). Black solid curve: metasurface with dimensions of $a = 2$ μm, $l = 1.45$ μm, and $w = 0.35$ μm; red dashed curve: metasurface with dimensions of $a = 2$ μm, $l = 1.7$ μm, and $w = 0.4$ μm; blue dotted curve: metasurface with dimensions of $a = 2.2$ μm, $l = 1.9$ μm, and $w = 0.4$ μm. (b) Retrieved effective surface impedance of metasurface with dimensions of $a = 2$ μm, $l = 1.45$ μm, and $w = 0.35$ μm ($245.41 - 29.73$j $\Omega/\square$ at wavelength 9.9 μm). (c) Retrieved effective surface impedance of metasurface with dimensions of $a = 2$ μm, $l = 1.7$ μm, and $w = 0.4$ μm ($247.06 - 174.02$j $\Omega/\square$ at wavelength 10.83 μm). (d) Retrieved effective surface impedance of metasurface with dimensions of $a = 2.2$ μm, $l = 1.9$ μm, and $w = 0.4$ μm ($139.12 - 169.61$j $\Omega/\square$ at wavelength 12.05 μm).

and $n_2 = 4$). Therefore, both metasurface absorbers achieve near-unity absorption, as shown in Fig. 5(a).

E-beam lithography and e-beam evaporator deposition processes were used to fabricate the metasurface absorber, starting with the deposition of 10/150 nm of Cr/Ag (mirror layer) on a silicon substrate, followed by the deposition of 600 nm of Ge (spacer layer) on the Ag mirror. After the e-beam lithography process, metal layer sequence of 3 nm Cr and 50 nm Ag was deposited. Finally, the lift-off process was used to form cross patterned metal. Fig. 6(b)–(d) show SEM images of the three different fabricated absorbers, whose dimensions are corresponding to those of the calculated absorbers as shown in Fig. 5. To characterize the spectral responses of the fabricated absorber, an FTIR microscope (Bruker Hyperion 3000) in reflectance mode at 4 cm^{-1} resolution was used to measure the spectral responses of the fabricated absorber after calibrating with a Ag mirror. Fig. 6(a) shows the measured spectral responses of the fabricated absorbers. Each of the wavelength-selective absorbers has an absorption peak at a wavelength of 9.4 μm with 89.4% (black solid), wavelength 10.54 μm with 97.57% (red dotted), and wavelength 11.84 μm with 93.25% (blue dashed). The small peaks at a wavelength of around 8 μm might be due to losses in the evaporated Ge layer. The results of the measured spectral responses are in good agreement with the results of the calculated spectral responses and show that this concept of the metasurface absorber is applicable to the microbolometer pixel.

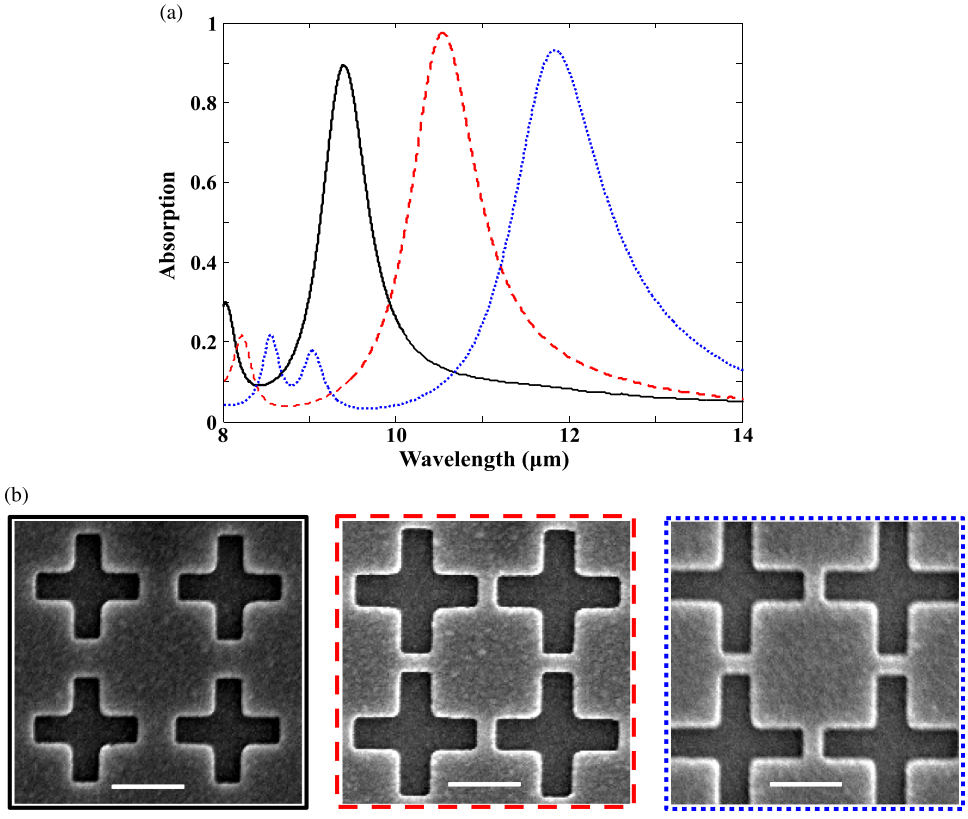

Fig. 6. (a) Measured spectral responses of three different wavelength-selective metasurface absorbers with a common Ge spacer layer thickness $(d = 0.6\ \mu\text{m})$ and metasurface thickness $(t_1 = 50\ \text{nm})$. Black solid curve: metasurface with dimensions of $a = 2\ \mu$m, $l = 1.45\ \mu$m, and $w = 0.35\ \mu$m; red dashed curve: metasurface with dimensions of $a = 2\ \mu$m, $l = 1.7\ \mu$m, and $w = 0.4\ \mu$m; blue dotted curve: metasurface with dimensions of $a = 2.2\ \mu$m, $l = 1.9\ \mu$m, and $w = 0.4\ \mu$m. (b) SEM images of the fabricated metasurface absorbers corresponding to black solid (left), red dashed (middle), and blue dotted curve (right). Scale bar is 1 μm.

As stated previously, thermally isolated absorbing membranes of a conventional microbolometer pixel mainly consist of a resistive absorbing layer, a temperature sensitive bolometric layer, and a mechanical support layer. Through the idea of our proposed metasurface absorber, the thin metal metasurface is able to be the resistive absorbing layer in the absorbing membranes of wavelength-selective microbolometer pixel. In a thermally isolated microbolometer structure the lossless Ge spacer layer would be replaced by the vacuum layer. The conceptual structure of the wavelength-selective microbolometer pixel, which is similar to that of the traditional amorphous silicon microbolometer pixel [32] except for the resistive absorbing layer, as shown in Fig. 7(a), is composed of suspended absorbing membranes consisting of an amorphous silicon (a-Si) bolometric and mechanical support layer (t_2) below the thin metal metasurface, air gap distance (d), and metal mirror layer. The dielectric a-Si layer is almost lossless and non-dispersive in the LWIR band and the refractive index of a-Si is assumed to be 3.42 [29]. To demonstrate the possibility of multispectral microbolometer focal plane arrays, the simulated spectral responses of three different conceptual structures of a wavelength-selective microbolometer pixel (i.e., structures have different wavelength selectivity), which have a common air gap distance d of 2 μm, a-Si thickness t_2 of 0.1 μm, and metasurface thickness t_1 of 50 nm, are shown in Fig. 7(b). Since the resonance wavelength of the metasurface is strongly influenced by the dielectric layer below the metasurface, the dimensions of the metasurface on the thin layer of amorphous silicon and the vacuum layer have to be adjusted. The dimensions of the metasurface for a peak wavelength around 9.15 μm (black solid) are $a = 4\ \mu$m, $l = 2.4\ \mu$m, and

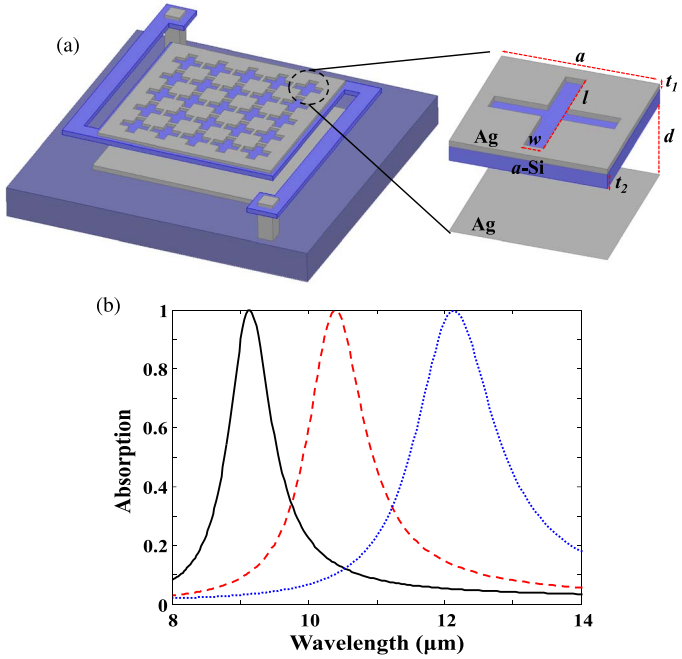

Fig. 7. (a) Schematic of the conceptual structure of a wavelength-selective microbolometer pixel based on a metasurface absorber. (b) Simulated spectral responses of three different wavelength-selective microbolometer pixels with a common air gap distance ($d = 2$ μm), metasurface thickness ($t_1 = 50$ nm), and a-Si thickness ($t_2 = 0.1$ μm). Black solid curve: metasurface with dimensions of $a = 4$ μm, $l = 2.4$ μm, and $w = 0.3$ μm; red dashed curve: metasurface with dimensions of $a = 4$ μm, $l = 2.7$ μm, and $w = 0.25$ μm; blue dotted curve: metasurface with dimensions of $a = 4$ μm, $l = 3.1$ μm, and $w = 0.2$ μm.

$w = 0.3$ μm; the dimensions of the metasurface for a peak wavelength around 10.4 μm (red dotted) are $a = 4$ μm, $l = 2.7$ μm, and $w = 0.25$ μm; the dimensions of the metasurface for a peak wavelength around 12.15 μm (blue dashed) are $a = 4$ μm, $l = 3.1$ μm, and $w = 0.2$ μm. Achievement of near-unity absorption of the three different pixels proves that this conceptual structure of a wavelength-selective microbolometer pixel can be an excellent candidate for multispectral microbolometer focal plane arrays. In contrast to the assumption of infinite periodicity used in the simulations, a pixel of a microbolometer would contain a finite array of unit cells. It has been shown that such array truncation of a metasurface in LWIR band causes the resonance wavelength shifts to the shorter wavelength with decreasing array size [33]. To counteract the effect of truncation array, the modified array of metasurface unit cells was applied [34]. When the pixel size of microbolometers with a metamaterial absorber is larger than the device operating wavelength, the metamaterial absorber produced excellent absorption [9]. Therefore, the size of pixel containing a finite array of unit cells for our conceptual structure should be larger than the device operating wavelength (14 μm), which is comparable with current microbolometer pixel size (sub-20 μm).

3. Conclusion

Wavelength-selective metasurface absorbers in the LWIR region are designed to be applicable to the structure of a multispectral microbolometer pixel. A single layer (50 nm) of a thin metal metasurface as an absorbing layer, which mainly dissipates the infrared absorption energy, is characterized through an effective surface impedance. The fabricated metasurface absorbers experimentally show efficient narrowband wavelength-selective absorption in the LWIR, and three-color spectral responses using different dimensions of the metasurface have been demonstrated. Therefore, the conceptual structure of a wavelength-selective microbolometer pixel

using our proposed metasurface absorber can be an excellent candidate for multispectral microbolometer focal plane arrays.

References

[1] J. J. Talghader, A. S. Gawarikar, and R. P. Shea, "Spectral selectivity in infrared thermal detection," *Light Sci. Appl.*, vol. 1, no. 8, p. e24, Aug. 2012.
[2] S.-W. Han, J.-W. Kim, Y.-S. Sohn, and D. P. Neikirk, "Design of infrared wavelength-selective microbolometers using planar multimode detectors," *Electron. Lett.*, vol. 40, no. 22, pp. 1410–1411, Oct. 2004.
[3] Y. Wang, B. J. Potter, and J. J. Talghader, "Coupled absorption filters for thermal detectors," *Opt. Lett.*, vol. 31, no. 13, pp. 1945–1947, Jul. 2006.
[4] J.-Y. Jung, J. Y. Park, S. Han, A. S. Weling, and D. P. Neikirk, "Wavelength-selective infrared Salisbury screen absorber," *Appl. Opt.*, vol. 53, no. 11, pp. 2431–2436, Apr. 2014.
[5] S. Ogawa, K. Okada, N. Fukushima, and M. Kimata, "Wavelength selective uncooled infrared sensor by plasmonics," *Appl. Phys. Lett.*, vol. 100, no. 2, Jan. 2012, Art. ID 021111.
[6] T. Maier and H. Brückl, "Wavelength-tunable microbolometers with metamaterial absorbers," *Opt. Lett.*, vol. 34, no. 19, pp. 3012–3014, Oct. 2009.
[7] T. Maier and H. Brueckl, "Multispectral microbolometers for the midinfrared," *Opt. Lett.*, vol. 35, no. 22, pp. 3766–3768, Nov. 2010.
[8] K. Du, Q. Li, W. Zhang, Y. Yang, and M. Qiu, "Wavelength and thermal distribution selectable microbolometers based on metamaterial absorbers," *IEEE Photon. J.*, vol. 7, no. 3, Jun. 2015, Art. ID 6800908.
[9] A. Tittl *et al.,* "A switchable mid-infrared plasmonic perfect absorber with multispectral thermal imaging capability," *Adv. Mater.*, vol. 27, no. 31, pp. 4597–4603, Aug. 2015.
[10] N. Landy, S. Sajuyigbe, J. Mock, D. Smith, and W. Padilla, "Perfect metamaterial absorber," *Phys. Rev. Lett.*, vol. 100, no. 20, May 2008, Art. ID 207402.
[11] N. Liu, M. Mesch, T. Weiss, M. Hentschel, and H. Giessen, "Infrared perfect absorber and its application as plasmonic sensor," *Nano Lett.*, vol. 10, no. 7, pp. 2342–2348, Jul. 2010.
[12] X. Liu, T. Starr, A. F. Starr, and W. J. Padilla, "Infrared spatial and frequency selective metamaterial with near-unity absorbance," *Phys. Rev. Lett.*, vol. 104, no. 20, May 2010, Art. ID 207403.
[13] C. Hu, X. Li, Q. Feng, X. N. Chen, and X. Luo, "Investigation on the role of the dielectric loss in metamaterial absorber," *Opt. Exp.*, vol. 18, no. 7, pp. 6598–6603, Mar. 2010.
[14] J. Hao *et al.,* "High performance optical absorber based on a plasmonic metamaterial," *Appl. Phys. Lett.*, vol. 96, no. 25, Jun. 2010, Art. ID 251104.
[15] Y. Chen, J. Dai, M. Yan, and M. Qiu, "Metal-insulator-metal plasmonic absorbers: Influence of lattice," *Opt. Exp.*, vol. 22, no. 25, pp. 30807–30814, Dec. 2014.
[16] A. V. Kildishev, A. Boltasseva, and V. M. Shalaev, "Planar photonics with metasurfaces," *Science*, vol. 339, no. 6125, Mar. 2013, Art. ID 1232009.
[17] N. Yu and F. Capasso, "Flat optics with designer metasurfaces," *Nature Mater.*, vol. 13, no. 2, pp. 139–150, Jan. 2014.
[18] P. Tassin, T. Koschny, and C. M. Soukoulis, "Effective material parameter retrieval for thin sheets: Theory and application to graphene, thin silver films, and single-layer metamaterials," *Physica B Condensed Matter*, vol. 407, no. 20, pp. 4062–4065, Oct. 2012.
[19] M. Unlu *et al.,* "Switchable scattering meta-surfaces for broadband terahertz modulation," *Sci. Rep.*, vol. 4, Jul. 2014, Art. ID 5708.
[20] X. Ni, A. V. Kildishev, and V. M. Shalaev, "Metasurface holograms for visible light," *Nature Commun.*, vol. 4, Nov. 2013, Art. ID 2807.
[21] N. Meinzer, W. L. Barnes, and I. R. Hooper, "Plasmonic meta-atoms and metasurfaces," *Nature Photon.*, vol. 8, no. 12, pp. 889–898, Nov. 2014.
[22] M. Pu *et al.,* "Design principles for infrared wide-angle perfect absorber based on plasmonic structure," *Opt. Exp.*, vol. 19, no. 18, pp. 17413–17420, Aug. 2011.
[23] Q. Feng, M. Pu, C. Hu, and X. Luo, "Engineering the dispersion of metamaterial surface for broadband infrared absorption," *Opt. Lett.*, vol. 37, no. 11, pp. 2133–2135, Jun. 2012.
[24] A. Andryieuski and A. V. Lavrinenko, "Graphene metamaterials based tunable terahertz absorber: Effective surface conductivity approach," *Opt. Exp.*, vol. 21, no. 7, pp. 9144–9155, Apr. 2013.
[25] Z. Wang *et al.,* "A circuit method to integrate metamaterial and graphene in absorber design," *Opt. Commun.*, vol. 329, pp. 76–80, Oct. 2014.
[26] Y. Yao *et al.,* "Electrically tunable metasurface perfect absorbers for ultrathin mid-infrared optical modulators," *Nano Lett.*, vol. 14, no. 11, pp. 6526–6532, Nov. 2014.
[27] Y. Fan, N.-H. Shen, T. Koschny, and C. M. Soukoulis, "Tunable terahertz meta-surface with graphene cut-wires," *ACS Photon.*, vol. 2, no. 1, pp. 151–156, Dec. 2015.
[28] B. Sensale-Rodriguez *et al.,* "Broadband graphene terahertz modulators enabled by intraband transitions," *Nat. Commun.*, vol. 3, Apr. 2012, Art. ID 780.
[29] E. D. Palik, *Handbook of Optical Constants of Solids*, vol. 1. New York, NY, USA: Academic, 1998.
[30] M. A. Ordal, R. J. Bell, R. Alexander, L. Long, and M. Querry, "Optical properties of fourteen metals in the infrared and far infrared: Al, Co, Cu, Au, Fe, Pb, Mo, Ni, Pd, Pt, Ag, Ti, V, and W," *Appl. Opt.*, vol. 24, no. 24, pp. 4493–4499, Dec. 1985.
[31] S. Zhang *et al.,* "Demonstration of metal-dielectric negative-index metamaterials with improved performance at optical frequencies," *J. Opt. Soc. Amer. B*, vol. 23, no. 3, pp. 434–438, Mar. 2006.

[32] J. Tissot, C. Trouilleau, B. Fieque, A. Crastes, and O. Legras, "Uncooled microbolometer detector: recent developments at ULIS," *Opto-Electron. Rev.*, vol. 49, no. 3, pp. 187–191, Jan. 2007.
[33] J. D'Archangel, E. Tucker, M. B. Raschke, and G. Boreman, "Array truncation effects in infrared frequency selective surfaces," *Opt. Exp.*, vol. 22, no. 13, pp. 16645–16659, Jun. 2014.
[34] J. A. D'Archangel, E. Z. Tucker, and G. D. Boreman, "Spectral modification of array truncation effects in infrared frequency selective surfaces," *Infrared Phys. Technol.*, vol. 71, pp. 285–288, Jul. 2015.